

AN INTRODUCTION TO 3D GLASS PRINTING

Grant Marchelli, Duane Storti, Mark Ganter, Renuka Prabhakar

Department of Mechanical Engineering, University of Washington, Seattle, WA 98195

Reviewed, accepted September 23, 2010

Abstract

This paper provides an overview of the process behind successfully adapting new materials, namely virgin glass and recycled glass, to 3D printing. The transition from 3DP ceramic systems to glass systems will be examined in detail, including, the necessary modifications to binder systems and printing parameters. We present preliminary engineering data on shrinkage and density as functions of peak firing temperature. In addition, we will provide a brief introduction to the complexities faced in realizing an adequate and repeatable firing method for printed glass.

1. Introduction

Adapting new materials to commercially available 3D powder printers is a time consuming and non-obvious development that requires experience and patience [1]. To successfully produce a 3D printed part using a non-stock powder system involves both careful monitoring and active modification of each parameter including, the materials' powder size and distribution, binder and binder activator formulation, layer thickness, printing saturation, and dry time.

History has defined man's most commonly used materials as wood, ceramic, metal, plastic, and glass [2]. Among these materials, wood, ceramic, metal, and plastic, have already been employed in Additive Manufacturing (AM) technologies [3]. Laminated Object Manufacturing (LOM) can use paper [4], Selective Laser Sintering (SLS) and 3DP can use metal [5] and ceramic [6-8], and Fused Deposition Modeling (FDM) uses plastic [9]. The remaining material, glass, while very similar to ceramic, has not been utilized by AM processes. For this reason, we have chosen glass as the next material for use in 3D printing.

New material systems for 3DP have been developed within the last few years, opening the doors to affordable 3DP [1]. Investigators used the stock powder systems as a starting point and eventually transitioned into new materials for 3DP, including ceramics [10]. Ceramics and glasses behave very similarly, but unlike many of the 3DP ceramics that readily absorb moisture, glass' hydrophobic nature yields a number of difficulties that arise during powder mixture and printing saturation optimization. Particle size and shape also play a pivotal role in realizing a 3DP glass part. Beyond the steps necessary to simply 3D print glass, are the tasks, developments, and post-processes required to produce a finished part. This paper will give the reader an overview and breakdown of the steps taken to create glass objects using commercial 3D printing hardware. We will also discuss the advantages and disadvantages of using virgin glass versus recycled glass, and present preliminary engineering data on shrinkage, porosity, and density as functions of peak firing temperature. Lastly, we will provide a brief introduction to the complexities involved with creating a repeatable firing method for 3D printed glass.

1.1 Binder formulation

In the past two decades, much effort has been placed into perfecting 3D printing and processing techniques for ceramic systems [1, 5-8, 10-13]. Recent developments have introduced organic binding agents into the powder system, which have opened the doors to affordable and flexible 3D printing. Glass' similarities to ceramics have provided an experimental baseline for developing an appropriate binder system for glass 3DP.

After outlining an experimental method to follow, it was necessary to find glass powder to be used in the experimentation. Virgin glass powder, or *frit*, was found at a local pottery supplier and was recommended

due to its uniformity. To determine the feasibility of using the virgin glass frit as a 3DP medium, we used the material systems presented by [10] and [13] as a foundation, and conducted a series of *spritz* tests. A *spritz* test is a simple, yet effective, method to verify powder and binder activator compatibility, as well as binding effectiveness, for new material systems as potential 3DP candidates. We started with the original ceramic mixture and substituted glass frit for ceramic powder. The powder mixture, comprised of 2/3 glass frit, 1/6 powdered sugar, and 1/6 maltodextrin, by weight [1, 10, 13], was placed in a small Petri dish and was *spritzed* with our binder activator consisting of water, alcohol, and food coloring. Ideally, the powder being tested should form a thin, but rigid shell on the topmost layer that was *spritzed*.

Unlike most clays, glass is hydrophobic, and so a gelatin-like shell was formed, as opposed to a crisp shell. Because the glass did not absorb any of the binder activator, the organic binding agents mixed with the glass powder became oversaturated and exhibited extremely long dry times, an undesirable result for 3DP systems. Realizing the glass mixture, in its current state, would be unfit for use in 3D printers, we carefully made adjustments to glass and organic binding agent ratios. An iterative process of *spritz* tests led to a mixture comprised of 4/5 glass frit, 1/10 powdered sugar, and 1/10 maltodextrin, by weight. The glass formulation provided significant reductions in powder binders (i.e., sugar and maltodextrin) when compared to the original ceramic mixtures. Because the glass was not absorbing the binder activator, we were able to reduce the amount of powder binder used in the formula, without comprising binding effectiveness.

1.2 Particle size

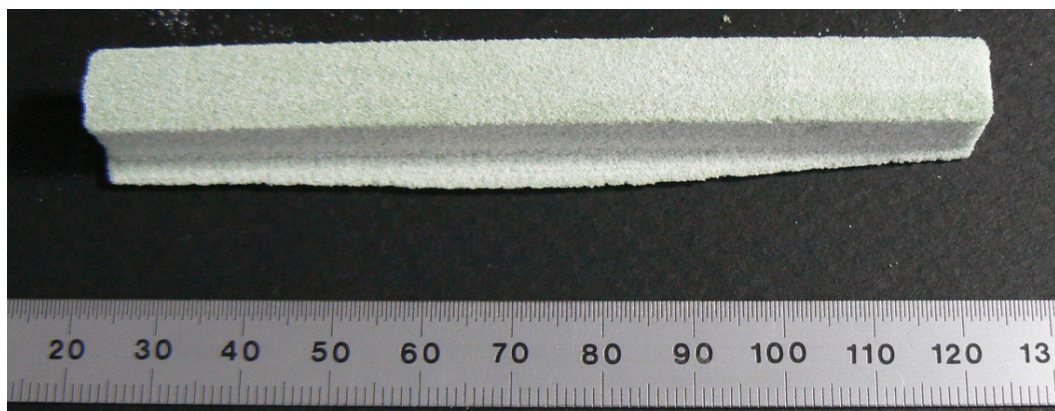
Successful adoption of new materials for 3DP requires powders with particle sizes in a limited range; ideal powders will possess particle sizes between 20-40 microns [1]. Studies have also shown success with 3DP of larger particles [8], but our initial experimentation utilized pre-sieved glass frit in the 20-40 micron particle size range. By using pre-sieved glass, as opposed to dry clay bodies, we were able to smoothly transition from the aforementioned ceramic system to the newly developed glass system, without having to modify printing parameters such as layer thickness.

Stock layer thicknesses are set at roughly 2-3 times the average particle size; a 20-40 micron powder mixture with a 30 micron average and Gaussian distribution is optimized when printed using approximately 100 micron (~0.004") layers. Excessive layer thickness will result in poor resolution and *stair-stepping* [3], whereas, insufficient layer thickness will produce inadequate powder spreading thereby leading to a lack of new material for successive cross-sections.



Figure 1: A specimen with highly pronounced layering resulting from the use of the large recycled glass particles. Specimen is as-printed.

Recycled glass powders with an average particle size of approximately 115 microns were also used during the experiment. We were limited to this particular particle size due to the inadequate pre-sieved, recycled glass powder supply, which will be explained in a subsequent section. Initial print tests with the larger particle size recycled glass powder system produced specimens with highly defined layering (see *Figure 1*). To accommodate the larger particle size powder, we used the maximum layer thickness permitted by the stock software, 215 microns ($\sim 0.008''$), which resulted in the highly defined layering. To alleviate the problem of low resolution without jeopardizing powder spread quality, we designed an iterative experiment that isolated layer thickness, by keeping all other printer and material parameters constant. Rectangular test specimens with dimensions of 10 mm x 10 mm x 100 mm were printed in various locations, and layer thickness was refined to accommodate the previous findings. During the experiment, we observed that with insufficient layer thicknesses equal to 100 microns, test specimens closest to the *feed reservoir* experienced disruption that we refer to as *swiping* (see *Figures 2*). As shown in *Figure 2*, swiping is demarked by the translation of the previously printed layer from its designated location as the next layer of powder is swept across the build bed. Swiping essentially destroys the part, leading to a failed build. A number of layer thickness tests were conducted, with each set of specimens being ranked on the severity of swiping. We determined that the most appropriate layer thickness for the recycled glass system was approximately 140 microns ($\sim 0.005''$), which supports reliable builds despite violating the usual rule of thumb that layer thickness should be about 3 times the particle size. Further investigation of particle size and its relation to layer thickness and spread quality is necessary.



a)



b)

Figure 2: a) Shows a top view of a standard 10 mm x 10 mm x 100 mm test specimen in the green state that has experienced swiping. b) Shows the side view of the same specimen with orientation inverted to make swiping visible. Notice the amount of layer dislocation occurring during swiping (~4 mm). The specimen is as-printed and scale is in millimeters.

1.3 Printing Saturation

Printing saturation is a parameter that includes two sub-variables: *shell* and *core*. Shell saturation refers to the volume of binder, or in our case binder activator, that is “ink-jetted” around the perimeter of the currently printing cross-section [6]. Core saturation refers to the volume of binder activator that is printed within the interior of the current cross-section. Stock software settings are optimized to produce crisp, fully adhered parts with minimal dry times for stock powders (typically based on plaster or starchplaster or starch). This requires a careful balance of shell and core saturation settings, with adverse ramifications if either setting is not optimized for the current powder/binder system.

Table 1 provides a list of the most common saturation combinations and the corresponding outcomes for ceramic and glass 3DP systems. We use this type of diagnostic table to determine when we need to increase or decrease the stock saturation settings. For example, we regularly print a set of test bars, allow them to dry, and break them in half. By analyzing the look and feel of both the shells and cores of the test

bars, we are able to categorize the current saturation settings, and make the necessary adjustments to reach *Case 5* characteristics.

Table 1: Shows how to identify the saturation state. Saturation can then be reduced or increased accordingly.

<i>Shell</i> <i>Core</i>	<i>Too Low</i>	<i>Appropriate</i>	<i>Too High</i>
<i>Too Low</i>	Case 1: Crumbles with contact pressure	Case 2: Good resolution; weak internal structure	Case 3: Swiping; weak internal structure
<i>Appropriate</i>	Case 4: Weak surface, strong internal structure	Case 5: Strong part; good resolution optimal dry time	Case 6: Swiping; poor resolution; strong part
<i>Too High</i>	Case 7: Poor resolution; weak surface; long dry time	Case 8: Swiping; strong part; long dry time;	Case 9: Gelatin-like; swiping; long dry time

Modifications to the shell and core saturations for glass required starting from the opposite corner of *Table 1*, when compared to the previously discussed ceramic systems [10, 13]. The dry clay bodies readily absorbed our binder activator, whereas the glass system was highly prone to oversaturation. The ceramic systems used in [13] typically exhibited *Case 1* attributes when we used stock saturation settings; the dry clay bodies used to create the powder absorb large amounts of binder activator, therefore, the shell and core saturations needed to be maximized in the 3DP software. If the saturation parameters were not providing enough binder activator per printing cycle, the resulting parts were not adequately adhered and crumbled upon contact. Insufficient saturation was remedied by sequentially increasing the saturation parameters until the parts behaved in a manner similar to *Case 5*. Glass on the other hand, required extreme reductions in saturation settings, pushing the limits of the 3DP software. Initially, the printed glass objects displayed *Case 9* attributes, and remained gelatin-like for up to five days. Careful refinement of the saturation settings, coupled with the previously optimized layer thickness parameter, led to high quality *Case 5*-like parts. The successfully 3D printed glass parts were still in the *green* or unfired state and were therefore strong enough to survive subsequent post-processing. It is worth noting that saturation settings will vary between printers, software editions, and environments (i.e., temperature and humidity). Saturation settings can be found at Open3D Printing (<http://open3dp.me.washington.edu/>). Post-processing the printed parts to increase strength will be discussed in the following section.

1.4 Post-processing

Glass parts created using 3D printing technologies can undergo post-processing techniques similar to those used for stock powder systems. Parts were infiltrated using paraffin wax to test the compatibility with 3DP glass. The infiltrated glass parts were comparable to infiltrated stock plaster parts, exhibiting large increases in strength and improvements in surface finish. Parts processed using paraffin wax as an infiltrant remain the same color as their unfired counterparts.

In addition, glass can be kiln-fired, much like clay systems, to sinter or fuse the lightly bound particles. We investigated two firing methods for 3DP glass; 1) direct firing, where the object is placed directly on the kiln-shelf, and 2) *setting*, where the object is partially or fully immersed in a medium, typically alumina.

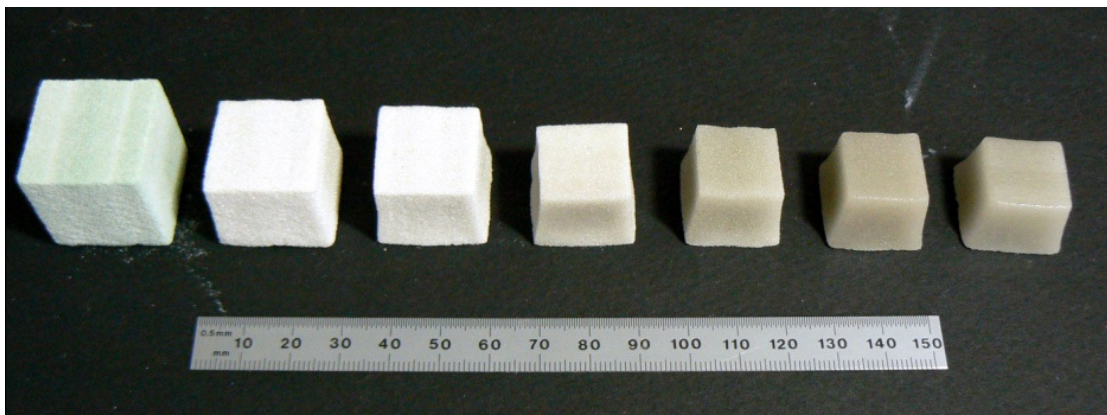


Figure 3: A set of 3DP recycled glass cubes ranging from as-printed on the left, to 99.64% dense on the right. Notice the anisotropic shrinkage behavior that becomes relevant starting with the center cube and moving rightwards. Scale is in millimeters.

Prior to firing, the kiln-shelves are prepared with a generic shelf primer to prevent sticking and to provide lubrication for the shrinking parts [14]. The parts resulting from the direct firing method take a variety of colors and surface textures, depending on the heating schedule and peak firing temperature as illustrated in *Figure 3*. The cubes on the left are relatively white and have a “sugar-cube” texture, whereas the cubes on the right are gray and have a more glass-like texture. The furthest cube on the left is *as-printed* or green, followed by cubes with ascending peak firing temperatures, ending with the rightmost cube fired at 760°C. Firing printed objects directly on the kiln-shelf typically increases the anisotropic shrinkage behavior, which can be seen in *Figure 7*. This phenomenon is a result of a temperature gradient within the kiln, as well as between the object and the shelf.

For this study, a simple, two-stage isothermal heating schedule was used to sinter the specimens (see *Figure 4*) [15-18]. The first stage of the heating schedule is used for binder burn-off, since the specimens were printed as a mixture of glass and organic binders (i.e., sugar, and maltodextrin). The organics will burn-off at relatively low temperatures between 200-500°C [18]. The kiln then ramps up to the peak firing temperature, where it is briefly held to allow for complete particle fusing, and then cooled naturally.

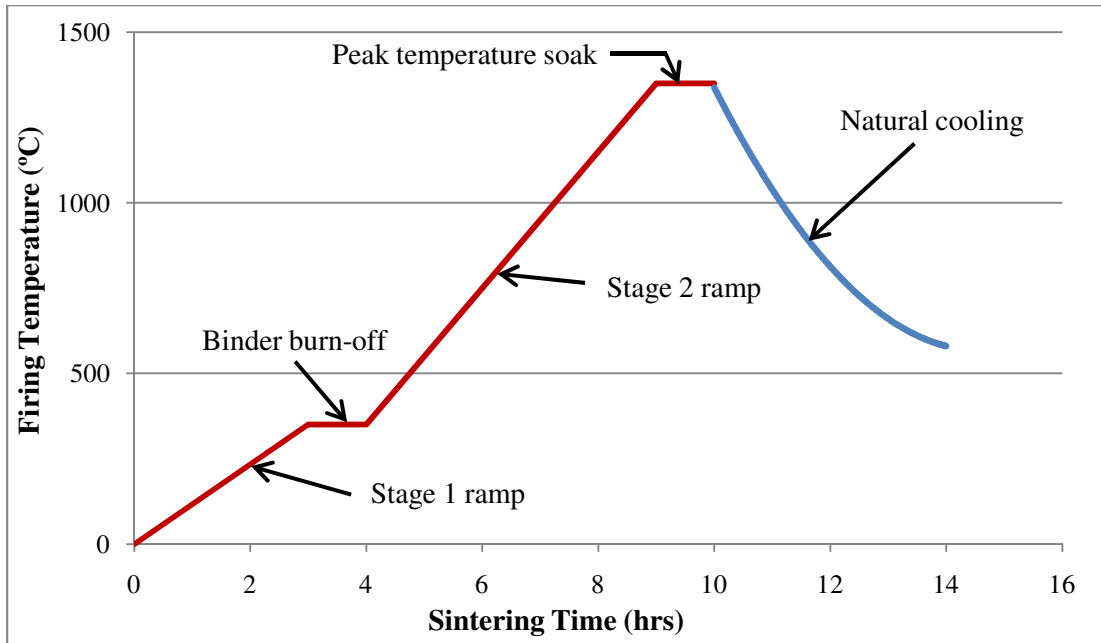


Figure 4: A generic version of the two-stage heating schedule used during experimentation. Ramp rates and holding temperatures will vary significantly between kilns and are therefore not published.

Setting is a firing method used for complex geometries that require support during the firing process. Parts are carefully immersed in a bed of setting medium, which is then placed into the kiln. The choice of setting medium depends on the desired surface finish and required firing temperatures. Alumina can take the form of powder, beads, or crystals, and has been implemented as our setting medium.

1.5 Virgin Versus Recycled Glass Powder

Experimentation with 3DP glass began with clear, virgin frit in the 20-40 micron range. Virgin glass was chosen because of an availability of material with optimal particle size distributions. Numerous retailers provide a wide variety of virgin glass frits; it can be purchased at nearly any particle size, allowing for an “off the shelf” constituent, with uniform and readily available properties.

In an effort to enable more environmentally conscious 3DP, we made the decision to experiment with recycled glass powders. Recycled glass powder can only be purchased in limited size ranges; typical distributors provide recycled glass in a macro size, making it difficult to source pre-sieved stock. Due to this limitation, we chose a pre-crushed recycled glass powder in the 40-200 micron range, as this was the closest to optimal powder we could purchase without crushing and sieving the recycled glass ourselves. Our development of glass 3DP sparked interest from industry, with recycled glass printing increasing curiosity. As a direct result of our research, industry professionals have exploited recycled glass as a printing medium with Shapeways (www.shapeways.com) recently providing commercial 3DP glass services, and EnVitrTM (www.envitrum.com) who uses 3DP recycled glass as a method to produce their prototypes for living systems.

Particle size greatly affects 3DP resolution, with larger particle creating less accurate parts and vice versa. For the purposes of this study, the lower resolution of the recycled glass powder did not pose a significant problem, but further testing has revealed great improvement on recycled glass resolution as a direct result of further optimization. *Figures 5 and 6* show a comparison of parts printed with virgin glass and recycled glass.

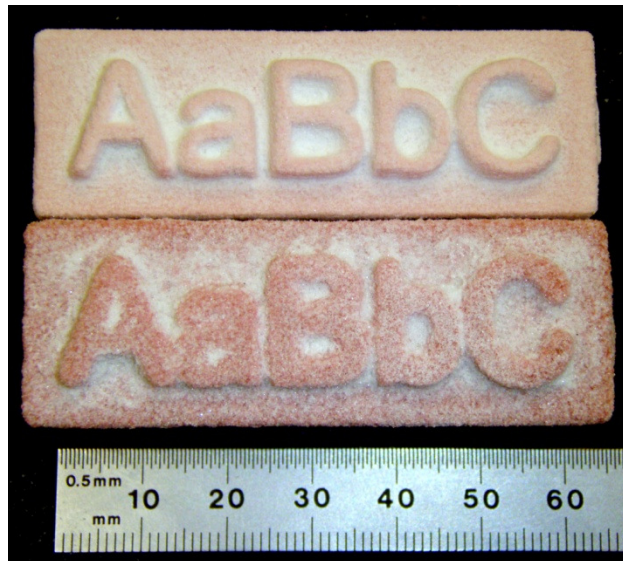
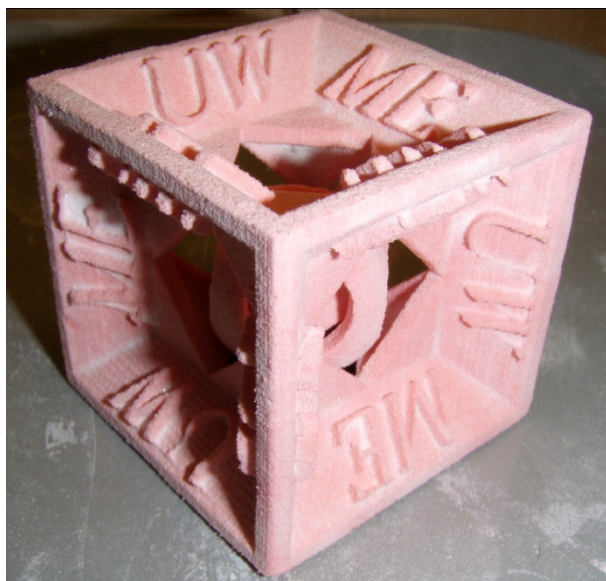


Figure 5: Above is printer diagnostics test with the virgin glass system. Below is the same resolution test using the recycled glass system. Notice the granular appearance of the recycled glass specimen, which is directly related to particle size. Both specimens are as-printed and scale is in millimeters.



a)



b)

Figure 6: The figures show photos of identical designs printed with virgin frit (a) and recycled glass (b). In both cases, complex geometries are successfully built, although the recycled glass parts show coarser resolution due to larger particle size and layer thickness.

Heating schedules for kiln-firings are also highly dependent on particle size; the firing optimization performed on the virgin frit was repeated to accommodate the larger recycled powder. In addition, most recycled glass powders are a combination of many different types of glass (i.e., plate, bottle, automotive,

etc.), which exhibit a range of sintering temperatures from 560°C to 960°C and characteristics including differences in shrinkage behavior [19].

The result of the 3DP compatibility and feasibility testing was the ability to 3DP in both virgin and recycled glass. The remainder of the paper will concentrate on the engineering testing conducted on the 3DP glass specimens for initial bulk property characterization.

2. Experimentation

Engineering strain, ε , defined as the change in length of a specimen divided by its original length, $\Delta L/L_0$, was determined for specimens fired at temperatures ranging from 691°C to 760°C in intervals of 4°C [20]. A total of 5 specimens per firing temperature with green dimensions of approximately 10 mm x 10 mm x 100 mm were printed and used in the experiment. The 100 mm length of the bar was printed in the *Fast-Axis* direction, with the remaining two 10 mm heights and widths being printed in the *Slow-Axis* and *Z-Axis* directions, respectively. This orientation was chosen for improved specimen green strength and was based on prior experimentation [13]. (Each specimen was measured at 3 different locations on the *Fast*-, *Slow*-, and *Z-Axes* before and after firing). Measurements were recorded using Mitutoyo digital calipers (ABSOLUTE DIGIMATIC), accurate to 0.01 mm. The Fast-Axis is defined as the direction traveled by the print head, the Slow-Axis is defined by the direction traveled by the gantry, and the Z-Axis is defined by the direction normal to the printed layers [6]. The results are shown in *Figure 7* and discussed in the subsequent section.

Specimens were fired at the same temperatures used during the shrinkage experiment and porosity was measured according to ASTM standard C373-88. This standard is written for ceramics, but since there are no ASTM standards for porous glass, we considered ASTM C373-88 to be the most applicable. After firing, specimens were dried to a constant dry mass D , and were then placed into a pan of distilled water and boiled for 5 hours. The specimens were then allowed to saturate in the distilled water for an additional 24 hours, to ensure complete impregnation of water into the interconnected micro-porous network. Using an *Archimedes* type testing apparatus, the specimens were weighed using an OHAUS® Adventurer™ scale, accurate to 0.001g, while suspended in a bath of distilled water, denoted as the suspended mass S . The saturated mass of the specimen M was then measured while weighing the specimen in air after patting the surface with a cloth to remove any excess water. The density of the water ρ_w was found to be 0.9982 at 19.8°C. Calculations for the apparent porosity P and the bulk density B were performed using the following equations [21]:

$$V = \frac{M - S}{\rho_w} \quad (1)$$

where, V is the exterior volume of the specimen, and M and S are previously defined as the saturated and suspended masses, respectively [13]. The apparent porosity P , defined as the relationship of the volume of open pores to the exterior volume of the specimen, was found using:

$$P = \left[\frac{M - D}{V} \right] \times 100 \quad (2)$$

where, M , D , and V are the saturated mass, dry mass, and exterior volume, respectively [21]. Using the apparent porosity P found in Eq. (2), the relative density ρ was found:

$$\rho = 1 - P \quad (3)$$

The bulk density B (g/cm^3) was then determined:

$$B = \frac{D}{V} \quad (4)$$

It is worth noting that the apparent porosity P can be expressed as a function of the saturated mass M , the exterior volume V , and the bulk density B :

$$P = \left[\frac{M}{V} - B \right] \times 100 \quad (5)$$

3. Results and Discussion

Shrinkage behavior for the 3D printed recycled glass showed significant anisotropy, especially beyond peak firing temperatures of 730°C, as seen in *Figure 7*. Shrinkage curves for each axis appear to follow a similar linear slope until approximately 746°C. Anisotropic shrink was pronounced at firing temperatures of 746°C and 760°C, with up to 23% differences in shrinkage between the Z-Axis and the Fast-Axis. At these firing temperatures, the glass particles began to vitrify and slump, which is indicated by the sudden changes in curve behavior for each axis. The linear curves for the Z-Axis, Slow-Axis, and Fast-Axis are presented below as Equations (6), (7), and (8), respectively:

$$\delta_z(T) = 0.4122T - 267.04 \quad (6)$$

$$\delta_s(T) = 0.3863T - 255.97 \quad (7)$$

$$\delta_f(T) = 0.2318T - 156.33 \quad (8)$$

where δ_i is shrinkage as a percentage, and T is the peak firing temperature in degrees Celsius. High coefficients of determination, R^2 , greater than 0.97 were found for all cases using the linear models, signifying good data representation. It is worth noting that peak firing temperatures at and above 760°C are beyond the range of the shrinkage sintering models and were excluded during curve fitting. This is due to the vitreous transition of the 3DP recycled glass at high temperatures.

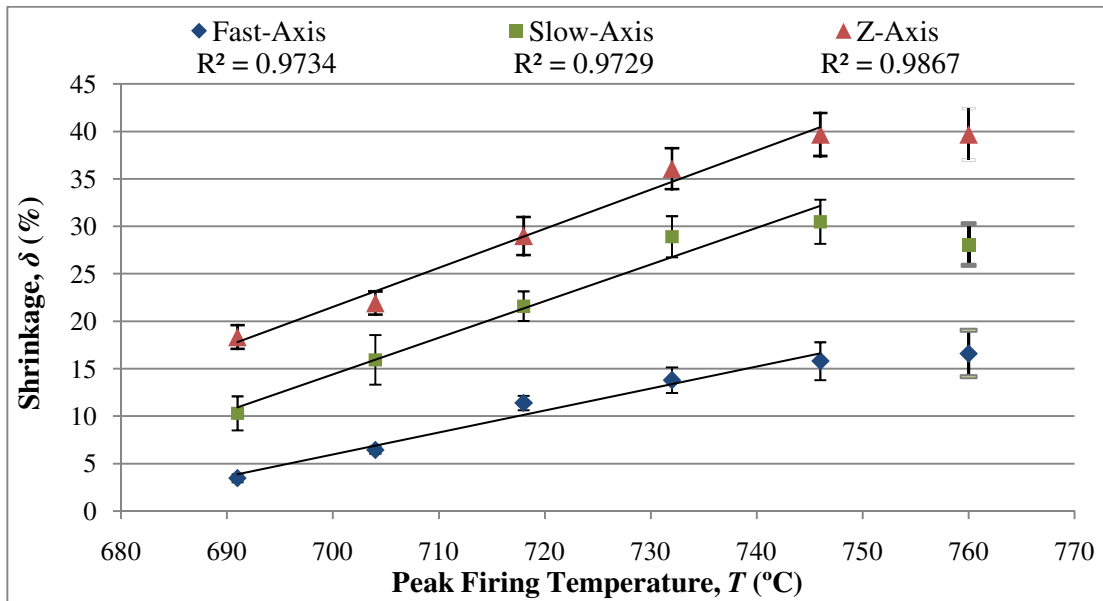


Figure 7: Recycled glass shrinkage as a function of peak firing temperature for the three printer axes. Notice the linear trends with high R^2 values. Beyond 746°C, the recycled glass begins to flow, and the model is no longer applicable.

Shrinkage for the Z-Axis leveled off at 39.68% and 39.69%, for firing temperatures of 746°C and 760°C, respectively. Slow-axis shrinkage decreased from 30.48% to 28.08% at 746°C and 760°C, respectively, showing a small expansion. This expansion was likely due to the slumping effect that occurs when glass reaches a threshold temperature known as the glass transition temperature T_G and begins to flow [19, 22].

Glass transition temperatures are typically within the range of 530°C to 1330°C, depending on the type of glass [23]. Fast-axis shrinkage increased from 15.79% to 16.59% at 746°C and 760°C, respectively, showing only a small decrease in shrinkage. In addition, Z-Axis shrinkage was by far the most profound, experiencing 6-11% and 15-23% more shrinkage over the range of firing temperatures than the Slow- and Fast-Axes, respectively. The average shrinkage ratios for the Slow- and Fast-Axes to the Z-Axis were 1:1.37 and 1:2.74, respectively. These extreme differences can be attributed to the layer-by-layer production method and binder burn-off.

Figure 8 shows the apparent porosity and bulk density data as a function of peak firing temperature. Linear fits produced limited R^2 values of less than 0.9 for both data sets, indicating that a higher order polynomial was needed to accurately fit the data. A quadratic fit was the simplest higher order polynomial alternative to a linear fit, and was used for both data sets, yielding R^2 values greater than 0.98. Apparent porosity P and bulk density B as quadratic functions of firing temperature in degrees Celsius T are given below as Equations (9) and (10), respectively:

$$P(T) = 0.0121T^2 - 18.311T + 6926 \quad (9)$$

and

$$B(T) = -0.0003T^2 + 0.4636T - 172.52 \quad (10)$$

It is worth noting that Equations (9) and (10) are dependent and related by Equation (5).

The apparent porosity for the 3DP glass was initially very high, 48.75% at a firing temperature of 691°C, but quickly decreased with increasing firing temperatures. At 760°C, the apparent porosity reached a minimum of 0.36%, indicating asymptotic behavior that approaches a fully dense 3DP glass specimen. At this temperature, the specimens exhibited smooth faces as the glass particles began to fully fuse together. The stair-stepping effect visible in specimens fired below 730°C, was no longer present, because the glass was beginning to flow within the kiln. Temperatures beyond 760°C were not explored due to the flowing nature of glass at high temperatures and the complete loss of recognizable shape that follows.

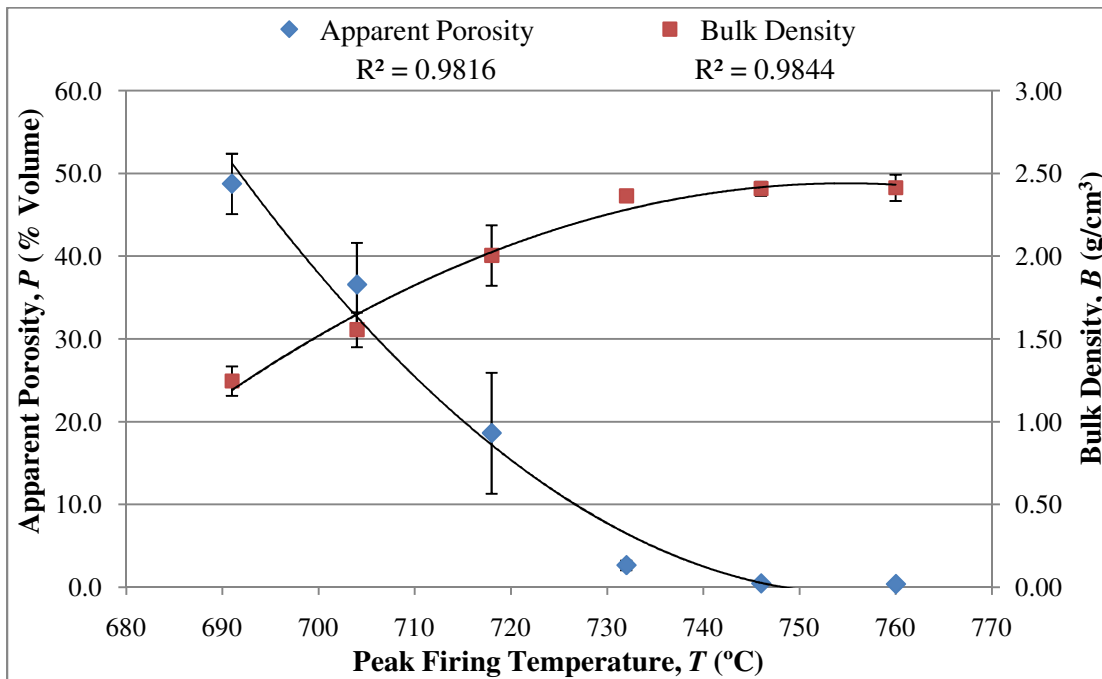


Figure 8: Recycled glass apparent porosity and bulk density as functions of peak firing temperature. The quadratic models yield high R^2 greater than 0.98.

Bulk densities ranging from 1.25 to 2.41 g/cm³ for firing temperatures of 691 to 760°C, respectively, were found. The bulk density of the 3DP glass also behaved in an asymptotic manner, appearing to approach a maximum of 2.41 g/cm³ for temperatures beyond 746°C. Bulk densities for common glass range from 2.4-2.8 g/cm³, demonstrating that the bulk density of our 3DP glass is within the accepted published range [24].

4. Conclusions

We have discussed the processes and methodologies behind adapting new materials, virgin and recycled glass, to powder-based 3DP systems. The transition from a ceramic to a novel glass material system for 3DP was developed by using the ceramic material system as a foundation for research. We included information on how to create the powder binder, which particle sizes are best suited for 3DP, and how to diagnose and optimize printing saturation. A preliminary two-stage heating schedule was also given and used for investigation of sintered bulk properties. Experimental data was presented for 3DP recycled glass including shrinkage, apparent porosity, and bulk density as functions of peak firing temperature. The shrinkage-temperature relation for 3DP recycled glass is well-approximated by a linear curve. At approximately 746°C, the glass begins to flow, thus the sintering models for shrinkage are applicable only for $T \geq 746^\circ\text{C}$. The 3DP recycled glass also exhibited significant anisotropy shrinkage behavior, with the Z-Axis shrinkage being the most prevalent, experiencing up to 23% more shrinkage than the Slow- and Fast-Axes. The average shrinkage ratios for the Slow- and Fast-Axes to the Z-Axis were 1:1.37 and 1:2.74, respectively. Anisotropic shrinkage behavior was likely a function of direct-shelf firing, coupled with the layer-by-layer production method; uncontrollable parameters such as print quality and powder mixture homogeneity would contribute to anisotropic behavior. The apparent porosity data was best approximated by an exponential fit, valid for sintering temperatures in the 690-760°C range. The bulk density data was best approximated by a quadratic fit. The apparent porosity was initially very high at 48.75% for low firing temperatures, but approached fully dense at 760°C. At low firing temperatures, the bulk density was slightly higher than room temperature water, but increased to a maximum of 2.41 g/cm³. This indicates that 3DP recycled glass can behave similarly to common glass with accepted published bulk densities ranging from 2.4-2.8 g/cm³. This research has enabled rapid manufacturing of recycled glass parts, giving rise to a sustainable future for 3DP.

5. Acknowledgements

The Solheim Rapid Manufacturing Laboratory would like to thank Roger Diehl from Saxton Bradley for lending us their Z-Corporation® ZPrinter® 310 Plus 3D printer for glass experimentation.

6. References

1. Utela, B., et al., *A review of process development steps for new material systems in three dimensional printing (3DP)*. Journal of Manufacturing Processes, 2008. **10**(2): p. 96-104.
2. Jester, T., *Twentieth Century Building Materials. History and Conservation*. Washington DC, 1995.
3. Gebhardt, A., *Rapid prototyping*. Munich; Cincinnati: Hanser Publishers, 2003. p. 47.
4. Mueller, B. and D. Kochan, *Laminated object manufacturing for rapid tooling and patternmaking in foundry industry*. Computers in Industry, 1999. **39**(1): p. 47-53.
5. Bourell, D.L., Marcus, H.L., Barlow, J.W., and Beaman, J.J. *Selective laser sintering of metals and ceramics*. International Journal of Powder Metallurgy, 1992. **10**(4): p. 369-381.
6. Sachs, E., et al., *Three-dimensional printing techniques*. U.S. Patent No. 5387380, Washington D.C.: U.S. Patent and Trademark Office, 1992.
7. Sachs, E., M. Cima, and J. Cornie, *Three-Dimensional Printing: Rapid Tooling and Prototypes Directly from a CAD Model*. CIRP Annals - Manufacturing Technology, 1990. **39**(1): p. 201-204.
8. Yoo, J., Cima, M.J., Khanuja, S., and Sachs, E.M. *Structural Ceramic Components by 3D Printing*. Proceedings of the Fourth International Solid Freeform Fabrication Symposium. Austin, TX: University of Texas, 1993.
9. Crump, S., *Apparatus and method for creating three-dimensional objects*. U.S. Patent No. 5121329, Washington D.C.: U.S. Patent and Trademark Office, 1989.
10. Ganter, M., Storti, D. and Utela, B. *The Printed Pot - Sometimes it's necessary to get outside the clay world to advance the field. In this case, three mechanical engineers print three-dimensional objects in clay, and they share their process and recipes*. Ceramics monthly, 2009. **57**(2): p. 36.
11. Cima, M. and E. Sachs. *Three dimensional printing: form, materials, and performance*. Proceedings of the Fifth International Solid Freeform Fabrication Symposium. Austin, TX: University of Texas, 1994.
12. Moon, J., Grau, J.E., Knezevic, V., Cima, M.J., and Sachs, E.M., *Ink-Jet Printing of Binders for Ceramic Components*. Journal of the American Ceramic Society, 2002. **85**(4): p. 755-762.
13. Marchelli, G., Ganter, M., and Storti, D. *New Material Systems for 3D Ceramic Printing*. Proceedings of the Twentieth International Solid Freeform Fabrication Symposium. Austin, TX: University of Texas.
14. Haun Labs, *Densification, Crystallization, and Sticking Behavior of Crushed Waste Glass Sintered in Refractory Molds with Release Agents*. CWC: Seattle, 2000.
15. G.C. Kuczynski. *Sintering processes*. Proceedings of the Fifth International Conference on Sintering and Related Phenomena. New York: Plenum Press, 1979.
16. German, R.M., *Sintering theory and practice*. New York: John Wiley & Sons, Inc., 1996. p. 8-12, 98-102, 335-338.
17. Rahaman, M.N., *Sintering of ceramics*. Boca Raton, FL: CRC Press, 2008. p. 1-6, 208-214, 305-335.
18. Johnston, S.R., *Initial stage sintering model of 316L stainless steel with application to three dimensionally printed (3DPTM) components*. Doctoral Dissertation: University of Washington, 2005. p. 10-11, 25-30.
19. Zarzycki, J., *Glasses and the vitreous state*. 1991, Cambridge: Cambridge university press.
20. Dowling, N., *Mechanical behavior of materials: engineering methods for deformation, fracture, and fatigue*. Upper Saddle River, NJ: Prentice Hall, 1993.
21. ASTM, Designation C373-88: *Standard Test Method for Water Absorption, Bulk Density, Apparent Porosity, and Apparent Specific Gravity of Fired Whiteware Products*. ASTM International: West Conshohocken, 2006.
22. Scholes, S., *Modern glass practice*. Chicago: Industrial Publications, 1951.
23. Le Bourhis, E., *Glass : mechanics and technology*. Weinheim: Wiley-VCH Verlag, 2008.
24. Giancoli, D.C., *Physics : principles with applications*. Upper Saddle River, NJ: Prentice Hall, 1998.